EEET ECOLOGICAL ENGINEERING & ENVIRONMENTAL TECHNOLOGY

Ecological Engineering & Environmental Technology, 2026, 27(8), 217–232
https://doi.org/10.12912/27197050/225184
ISSN 2719–7050, License CC-BY 4.0

Received: 2026.06.16
Accepted: 2026.07.10
Published: 2026.08.01

Spatiotemporal dynamics of land cover before, during, and after the earthquake, using Sentinel-2 imagery and random forest classification

Laela Indawati[1,2], Prabang Setyono[3], Nur Hafidha Hikmayani[4], Ari Probandari[5*]

[1] Postgraduate School, Universitas Sebelas Maret, Ir. Sutami Street, 57126 Surakarta, Indonesia
[2] Department of Medical Record and Health Information, Faculty of Health Sciences, Universitas Esa Unggul, Arjuna Utara Street, West Jakarta 11510, Indonesia
[3] Postgraduate School, Universitas Sebelas Maret, Surakarta 57126, Central Java, Indonesia,
[4] Department of Pharmacology, Faculty of Medicine, Universitas Sebelas Maret, Surakarta 57126, Central Java, Indonesia
[5] Department of Public Health, Faculty of Medicine, Universitas Sebelas Maret, Surakarta 57126, Central Java, Indonesia
* Corresponding author's e-mail: ari.probandari@staff.uns.ac.id

ABSTRACT

This study aimed to analyze the spatiotemporal dynamics of land cover in Cianjur Regency, Indonesia, before (2021), during (2022), and after (2023) the 2022 earthquake, using multitemporal Sentinel-2 imagery and a Random Forest classifier implemented in Google Earth Engine. Six Sentinel-2 spectral bands and six spectral indices (NDVI, EVI, mNDWI, NDBI, NDBaI, and NBR) were used as classification variables. Land cover was classified into six major classes, namely built-up land, water bodies, wet agricultural land, open land, secondary dryland forest, and mixed dryland agriculture and shrubland. Accuracy assessment yielded overall accuracy values ranging from 72.12% to 83.65%, with kappa coefficients indicating substantial agreement. The results revealed that secondary dryland forest remained the dominant land cover class but decreased consistently from 236,170.58 ha in 2021 to 217,503.11 ha in 2023. During the earthquake year, land cover changes were characterized by increased open land and reduced vegetation cover, whereas the post-earthquake period was marked by significant increases in built-up land and wet agricultural land accompanied by a decline in open land. Spatial analysis indicated that land cover changes were more intensive in the northern part of Cianjur Regency, where the earthquake epicenter and major settlement areas were located. The findings suggest that post-earthquake landscape transformation occurred through two distinct phases, namely a disturbance phase during the earthquake year and a reorganization phase during the recovery period. This study highlights the importance of multitemporal remote sensing approaches for capturing post-disaster landscape dynamics and provides valuable information for environmental rehabilitation, spatial planning, and disaster risk reduction.

Keywords: land cover change, earthquake, spatiotemporal analysis, Sentinel-2, Google Earth Engine, random forest, regency.

INTRODUCTION

Earthquakes are among the most destructive geological disasters because they not only cause casualties and damage to infrastructure but also trigger long-term environmental changes (Civelek et al., 2023). These environmental impacts include surface deformation (Civelek et al., 2023), landslides (Yang et al., 2018), alterations in hydrological systems, vegetation damage (Caja et al., 2018), and land cover transformation that may affect ecosystem stability and ecological functions (Sidle et al., 2018). Therefore, understanding post-disaster landscape changes is important to support environmental rehabilitation, regional management, and disaster risk reduction in the future.

On November 21, 2022, a Mw 5.6 earthquake struck Cianjur Regency, West Java Province, Indonesia, causing extensive damage to settlements, infrastructure, and the surrounding environment (Arwasaputra et al., 2024; Zulfakriza et al., 2024). The earthquake was followed by hundreds of aftershocks and triggered various hazards, especially landslides in hilly and mountainous areas. Several studies have reported that the earthquake caused surface deformation in the form of subsidence and uplift, which altered local geomorphological conditions and increased the potential for secondary geological hazards (Awaluddin, 2026; Hadmoko et al., 2024). These findings suggest that earthquake impacts are not limited to immediate physical damage but may also trigger long-term changes in landscape characteristics and environmental dynamics.

The development of remote sensing technology has opened up opportunities to monitor environmental changes due to disasters more effectively (Mashala et al., 2023). Sentinel-2 imagery is widely used for land cover mapping because its high spatial and temporal resolution enables effective monitoring of changes in land surface conditions (Noi Phan et al., 2020; Phiri et al., 2020). In addition, machine-learning algorithms, particularly Random Forest, have been shown to improve land cover classification accuracy because they can model complex nonlinear relationships and integrate multiple spectral variables simultaneously (Adugna et al., 2022; Sousa et al., 2020).

Although research related to the 2022 earthquake has expanded considerably, most studies have focused on building damage, surface deformation, landslide hazards, relocation planning, and disaster-risk financing (Handoyo et al., 2024; Zulfakriza et al., 2024). Existing remote-sensing studies have generally adopted a before–after approach to assess environmental changes associated with the earthquake. For example, Prayogo (2023) used Sentinel-2 imagery to analyze changes in land cover and building density before and after the earthquake, but the analysis was only carried out in two observation periods with relatively simple land cover classifications (Prayogo, 2023). As a result, the dynamics of landscape change that took place during the year of the earthquake and the period after it could not be comprehensively explained.

Despite these efforts, a knowledge gap remains regarding how land cover in Cianjur Regency changed spatially and temporally before, during, and after the 2022 earthquake. Most previous studies relied on a before–after framework that primarily captured the immediate impacts of the disaster and therefore could not fully explain landscape dynamics over multiple years. In addition, research that integrates multitemporal Sentinel-2 imagery, various spectral indices, and Random Forest algorithms to evaluate land cover changes at the scale of Cianjur Regency is still very limited.

Based on these gaps, this study aims to analyze the spatial and temporal dynamics of land cover in Cianjur Regency before, during, and after the 2022 earthquake using Sentinel-2 imagery and the Random Forest algorithm on the Google Earth Engine platform. Specifically, this study aimed to: (1) map the condition of land cover in 2021, 2022, and 2023; (2) identify changes in the extent of each land cover class during the observation period; and (3) evaluate the pattern of land cover changes that occurred in the period before, during, and after the earthquake.

The novelty of this study lies in the application of a multitemporal approach to evaluate land cover dynamics across three observation periods: before the earthquake (2021), during the earthquake year (2022), and after the earthquake (2023). In addition, this study integrates Sentinel-2 spectral bands, multiple spectral indices, and the Random Forest algorithm to generate a detailed land cover classification.

Unlike previous studies that primarily adopted a conventional before–after framework to assess disaster impacts, this study examines sequential land cover changes over three consecutive years. This approach enables the identification of landscape dynamics that occur not only during the disaster year but also throughout the post-disaster recovery period.

The findings contribute to a more comprehensive understanding of post-earthquake landscape transformation in Cianjur Regency. Furthermore, the results provide geospatial information that may support environmental rehabilitation planning, land-use management, and disaster risk reduction efforts in earthquake-prone regions.

METHODS

Study area

The study was conducted in Cianjur Regency, West Java Province, Indonesia, located between

106°42′–107°25′ E and 6°21′–7°25′ S. Covering approximately 359,460 ha, the regency is characterized by mountainous and hilly terrain, extensive agricultural land, and forested areas. On November 21, 2022, the region was struck by a Mw 5.6 earthquake that caused extensive damage to settlements, infrastructure, and the surrounding environment, making it a suitable case study for evaluating post-disaster land cover dynamics.

Sentinel-2 data acquisition and pre-processing

This study used harmonized Sentinel-2 MultiSpectral Instrument (MSI) Level-2A data available through the Google Earth Engine (GEE) platform. Three annual composite images were generated to represent land cover conditions before the earthquake (2021), during the earthquake year (2022), and after the earthquake (2023). The January–November period was selected to ensure temporal consistency among observation years while minimizing the influence of seasonal variability and persistent cloud cover commonly associated with the peak rainy season. Image pre-processing included cloud masking, median compositing, and image clipping based on the study-area boundary. All processing steps were performed within the Google Earth Engine platform. Sentinel-2 imagery was selected because it offers high spatial resolution (10–20 m), frequent revisit intervals, and open access, making it well suited for monitoring regional-scale land cover dynamics.

Spectral variable development

In addition to Sentinel-2 spectral bands, several spectral indices were used as supplementary variables to improve the discrimination of land cover classes. The indices included the normalized difference vegetation index (NDVI), enhanced vegetation index (EVI), modified normalized difference water index (mNDWI), normalized difference built-up index (NDBI), normalized difference bareness index (NDBaI), and normalized burn ratio (NBR).

These indices were derived from combinations of Sentinel-2 spectral bands and subsequently integrated with the original spectral bands through a layer-stacking process. The final dataset consisted of six Sentinel-2 spectral bands (blue, green, red, near infrared [NIR], shortwave infrared 1 [SWIR-1], and shortwave infrared 2 [SWIR-2]) and six spectral indices, which were used as input variables for land cover classification. Table 1 summarizes the formulas of the spectral indices used in this study.

Training and validation samples

Training and validation samples were obtained through visual interpretation of high-resolution imagery from Google Earth Pro and NICFI Planet Basemaps. Based on the dominant land-cover characteristics of the study area, seven land-cover classes were defined: built-up land, water bodies, wet agricultural land, open land, secondary dryland forest, mixed dryland agriculture and shrubland, and cloud/shadow (no-data) areas.

The cloud/shadow class was included to account for pixels affected by residual cloud contamination and cloud shadows that remained after image pre-processing. Although this class was retained during classification to ensure complete spatial coverage and consistency in area estimation, it was excluded from the interpretation of land-cover dynamics because it does not represent an actual land-cover category.

Samples were collected as polygons representing homogeneous areas within each land-cover class. This approach was adopted to capture within-class spectral variability while minimizing the influence of mixed pixels. To reduce spatial

Table 1. Spectral indices derived from Sentinel-2 imagery and used in the classification process

Spectral Index	Formula	Reference
NDVI	(NIR − Red)/(NIR + Red)	Phan et al. (2020)
EVI	2.5 × ((NIR − Red)/(NIR + 6Red − 7.5Blue + 1))	Liu and Huete (1995)
mNDWI	(Green − SWIR1)/(Green + SWIR1)	Xu (2006)
NDBI	(SWIR1 − NIR)/(SWIR1 + NIR)	Zha et al. (2003)
NDBaI	(SWIR1 − SWIR2)/(SWIR1 + SWIR2)	Li and Chen (2014)
NBR	(NIR − SWIR2)/(NIR + SWIR2)	Key and Benson (2006)

autocorrelation, a minimum distance of 100 m was maintained between training and validation samples, following recommendations from previous land-cover classification studies.

A total of 456 samples were collected and randomly divided into training and validation datasets. Of these, 75% were allocated for model training and 25% for validation. This allocation was selected to provide a balance between classifier development and independent accuracy assessment while ensuring sufficient samples for both purposes. A total of 104 validation samples were used for each observation year (2021, 2022, and 2023) to evaluate classification performance.

Land cover classification using random forest

Random Forest was selected for its ability to handle multivariate data, its resistance to overfitting, and its consistently high classification accuracy in remote sensing–based land-cover mapping applications (Breiman, 2001; Phan et al., 2020; Magidi et al., 2021).

The input variables consisted of Sentinel-2 spectral bands and the spectral indices derived during the pre-processing stage. The resulting classifications were used to generate land cover maps of Regency for 2021, 2022, and 2023, which subsequently served as the basis for analyzing spatiotemporal land cover dynamics.

Accuracy assessment

Classification performance was evaluated using a confusion matrix based on the validation dataset. The assessment metrics included producer's accuracy (PA), user's accuracy (UA), overall accuracy (OA), and the kappa coefficient. Overall accuracy was used to quantify the proportion of correctly classified samples, whereas the kappa coefficient was used to assess the level of agreement between the classification results and the reference data after accounting for agreement occurring by chance. The interpretation of kappa values followed the classification proposed by Viera and Garrett (2005).

Spatiotemporal land cover dynamics analysis

Land cover dynamics were analyzed by comparing classification results from 2021, 2022, and 2023. The area of each land cover class was calculated in hectares and compared across observation periods to identify changes occurring before, during, and after the 2022 Earthquake. The rate of land cover change was calculated using Equation 1:

$$V = \frac{N_2 - N_1}{N_1} \times 100 \quad (1)$$

where: V – rate of land cover change (%), $N1$ – land cover area in the initial period (ha), $N2$ – land cover area in the subsequent period (ha).

The analysis was conducted for two time intervals: 2021–2022 and 2022–2023. The first interval represented the transition from pre-earthquake conditions to the earthquake year, whereas the second represented changes occurring during the post-earthquake period. The cloud/shadow (no-data) class was excluded from the interpretation of land cover change because it did not represent a physical land cover category.

Analytical framework

The analysis was conducted in three main stages. First, land cover classification was performed to generate land cover maps for 2021, 2022, and 2023. Second, the area of each land cover class was calculated for each observation year. Third, changes in land cover area and rates of change were analyzed by comparing the 2021–2022 and 2022–2023 periods to identify land cover dynamics before, during, and after the 2022 Earthquake.

The overall workflow consisted of Sentinel-2 data acquisition, image pre-processing, spectral index calculation, Random Forest classification, accuracy assessment, and analysis of multitemporal land cover dynamics, as illustrated in Figure 1.

RESULTS

Classification accuracy assessment

The Random Forest classifier produced satisfactory classification results across all observation years (Table 2). Overall accuracy (OA) values were 83.65%, 72.12%, and 75.00% for 2021, 2022, and 2023, respectively. The corresponding kappa coefficients ranged from 64.28% to 77.03%. Based on the classification proposed by Viera and Garrett (Viera and Garrett, 2005), all kappa values were classified as substantial agreement, indicating good agreement between the classified maps

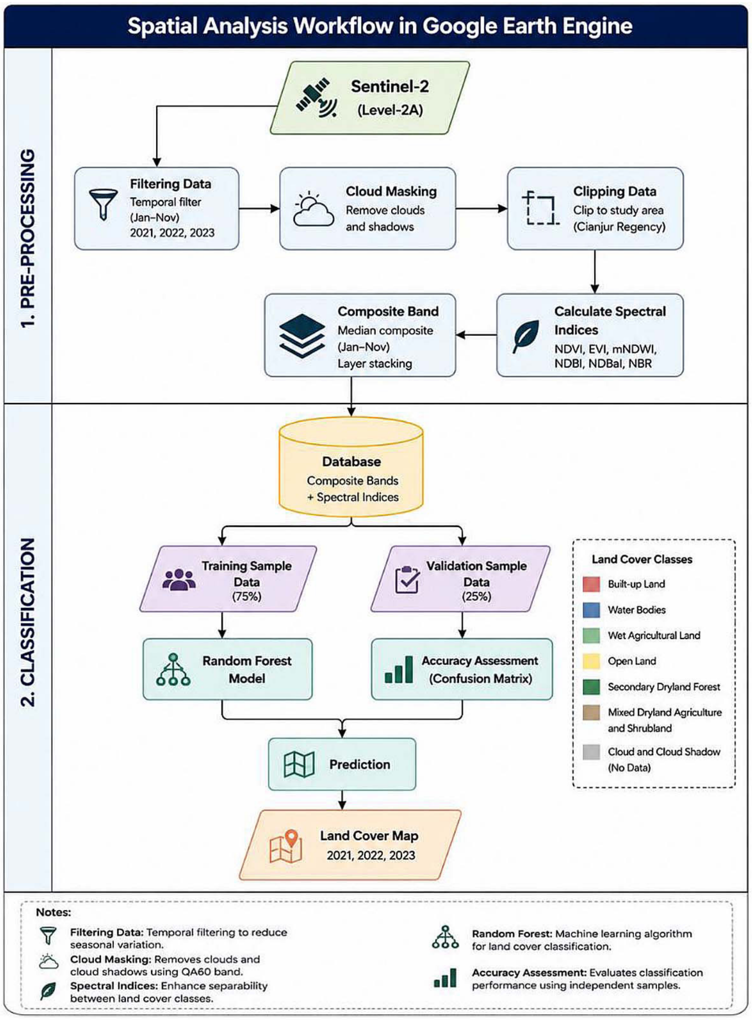

Figure 1. Workflow of multi-temporal land cover classification and spatiotemporal dynamics analysis using Sentinel-2 imagery and Random Forest in Google Earth Engine

and the reference data. The class-specific accuracy assessment revealed variations among land cover classes (Table 3). Secondary dryland forest consistently exhibited high classification performance throughout the study period, with Producer's Accuracy ranging from 80.8% to 86.3% and user's accuracy ranging from 78.1% to 97.8%. In contrast, wet agricultural land showed relatively lower accuracy, particularly in 2022 and 2023.

Table 2. Overall accuracy and kappa statistics

Year	Overall accuracy (%)	Kappa (%)	Agreement
2021	83.65	77.03	Substantial
2022	72.12	64.28	Substantial
2023	75.00	65.09	Substantial

Land cover distribution before the earthquake (2021)

The 2021 land cover map represented baseline land cover conditions prior to the 2022 Earthquake (Table 4). Secondary dryland forest was the dominant land cover class, covering 236,170.58 ha or 65.70% of the study area. Mixed dryland agriculture and shrubland was the second largest class, occupying 69,086.84 ha (19.22%), followed by wet agricultural land covering 39,471.04 ha (10.98%). Built-up land covered 10,533.13 ha (2.93%) of the study area, while open land and water bodies occupied 2,543.28 ha (0.71%) and 1,151.40 ha (0.32%), respectively. Overall, secondary dryland forest and agricultural land classes accounted for more than 95% of the total study area in 2021.

Figure 2 shows that secondary dryland forest was widely distributed across the central, southern, and southeastern parts of Cianjur Regency. Forest cover formed extensive vegetation patches

Table 3. Producer's accuracy (PA) and user's accuracy (UA) of land cover classes

Land cover class	PA 2021 (%)	UA 2021 (%)	PA 2022 (%)	UA 2022 (%)	PA 2023 (%)	UA 2023 (%)
Built-up land	100.0	80.0	100.0	81.8	66.7	84.2
Water bodies	100.0	50.0	75.0	85.7	100.0	50.0
Wet agricultural land	61.5	80.0	77.8	43.8	57.1	33.3
Open land	50.0	50.0	62.5	62.5	75.0	75.0
Secondary dryland forest	86.3	97.8	82.1	78.1	80.8	97.7
Mixed dryland agriculture & shrubland	90.0	75.0	80.0	80.0	76.9	50.0

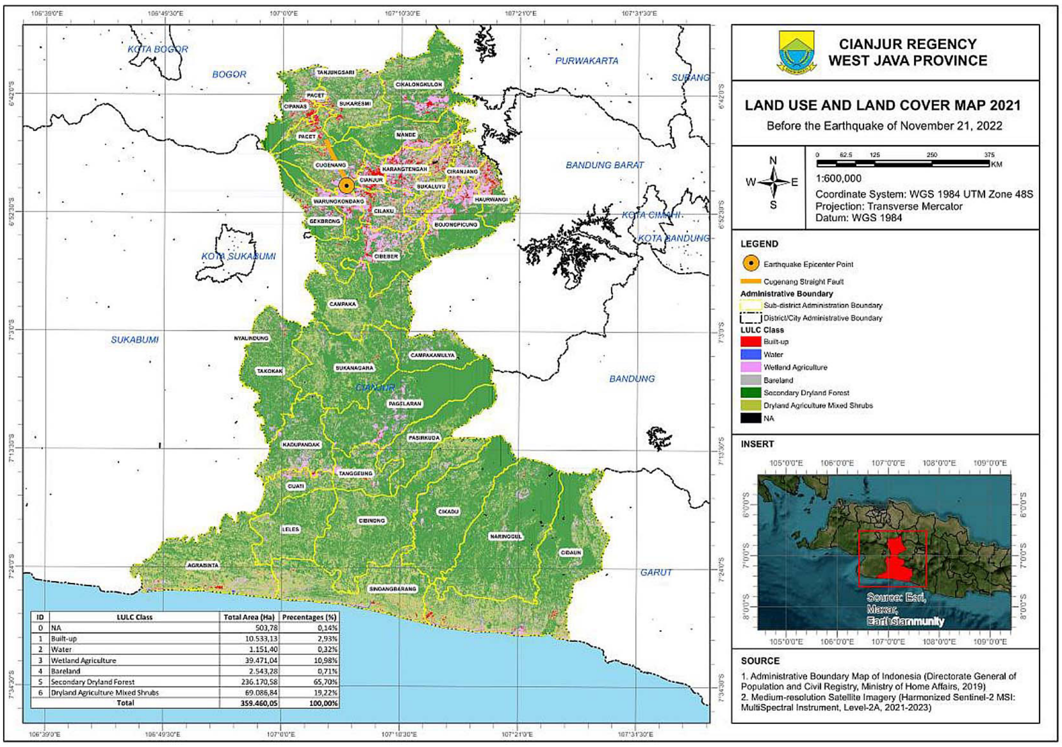

Figure 2. Land cover distribution in regency in 2021

Table 4. Land cover distribution in Cianjur Regency before the 2022 earthquake (2021)

ID	Land cover class	Area (ha)	Percentage (%)
0	No data (cloud/shadow)	503.78	0.14
1	Built-up land	10,533.13	2.93
2	Water bodies	1,151.40	0.32
3	Wet agricultural land	39,471.04	10.98
4	Open land	2,543.28	0.71
5	Secondary dryland forest	236,170.58	65.70
6	Mixed dryland agriculture and shrubland	69,086.84	19.22
Total		359,460.05	100.00

with relatively low fragmentation and constituted the dominant land cover type in 2021. Mixed dryland agriculture and shrubland were mainly distributed in transition zones between forested and cultivated areas, particularly in the central part of the regency.

Meanwhile, wet agricultural land was concentrated in relatively flat areas and valleys in the northern and central regions. Built-up land exhibited a clustered distribution pattern around urban centers and settlements, especially in the northern part of Cianjur Regency, whereas open land and water bodies occupied relatively small and scattered areas. The earthquake epicenter was located in the northern part of the regency, where agricultural land, settlements, and secondary vegetation formed a heterogeneous landscape mosaic.

Land cover distribution during the earthquake year (2022)

The 2022 land cover map showed changes in land cover composition compared with pre-earthquake conditions (Table 5). Secondary dryland forest remained the dominant land cover class, covering 229,525.73 ha or 63.85% of the study area. Mixed dryland agriculture and shrubland occupied 75,845.60 ha (21.10%), while wet agricultural land covered 25,365.33 ha (7.06%).

Built-up land accounted for 7,387.78 ha (2.06%) of the study area. Open land increased to 4,123.22 ha (1.15%), whereas water bodies occupied 1,768.52 ha (0.49%). Compared with 2021, the extent of secondary dryland forest and wet agricultural land decreased, while open land, water bodies, and mixed dryland agriculture and shrubland increased in 2022.

The 2022 land cover map (Figure 3) showed that secondary dryland forest remained the dominant land cover class and was widely distributed across the central, southern, and southeastern parts of Cianjur Regency. Forest cover continued to form extensive vegetation patches with relatively low fragmentation, although localized fragmentation was observed in some areas due to the presence of other land cover classes.

Mixed dryland agriculture and shrubland were generally distributed in transition zones between forested and cultivated areas, particularly in the central region. Meanwhile, wet agricultural land remained concentrated in relatively flat areas in the northern and central parts of the study area. Built-up land exhibited a clustered distribution pattern around urban areas and settlement centers, especially in northern Regency.

In addition, no-data areas associated with clouds and cloud shadows were observed in several parts of the study area, particularly in the central and southeastern sectors. Consequently, the proportion of the no-data class was greater in 2022 than in 2021.

Land cover distribution after the earthquake (2023)

The 2023 land cover map revealed a different land cover composition compared with the previous observation years (Table 6). Secondary dryland forest remained the dominant land cover class, covering 217,503.11 ha or 60.51% of the study area. Mixed dryland agriculture and shrubland represented the second largest class, occupying 61,275.83 ha (17.05%), followed by wet agricultural land covering 43,318.10 ha (12.05%).

Built-up land increased to 34,437.11 ha (9.58%), whereas open land accounted for only 2,125.48 ha (0.59%) of the study area. Water bodies occupied 799.46 ha (0.22%), representing the smallest land cover class in 2023. Overall, forest and agricultural land classes remained the dominant land cover categories in Regency, accounting for more than 89% of the total study area.

In contrast to conditions in 2022, Figure 4 showed a clearer land cover distribution pattern, with almost no areas classified as no-data. Secondary dryland forest remained dominant across most of Cianjur Regency, particularly in the central, southern, and southeastern regions, where

Table 5. Land cover distribution in Cianjur Regency during the earthquake year (2022)

ID	Land cover class	Area (ha)	Percentage (%)
0	No data (cloud/shadow)	15,443.49	4.30
1	Built-up land	7,387.78	2.06
2	Water bodies	1,768.52	0.49
3	Wet agricultural land	25,365.33	7.06
4	Open land	4,123.22	1.15
5	Secondary dryland forest	229,525.73	63.85
6	Mixed dryland agriculture and shrubland	75,845.60	21.10
Total		359,459.66	100.00

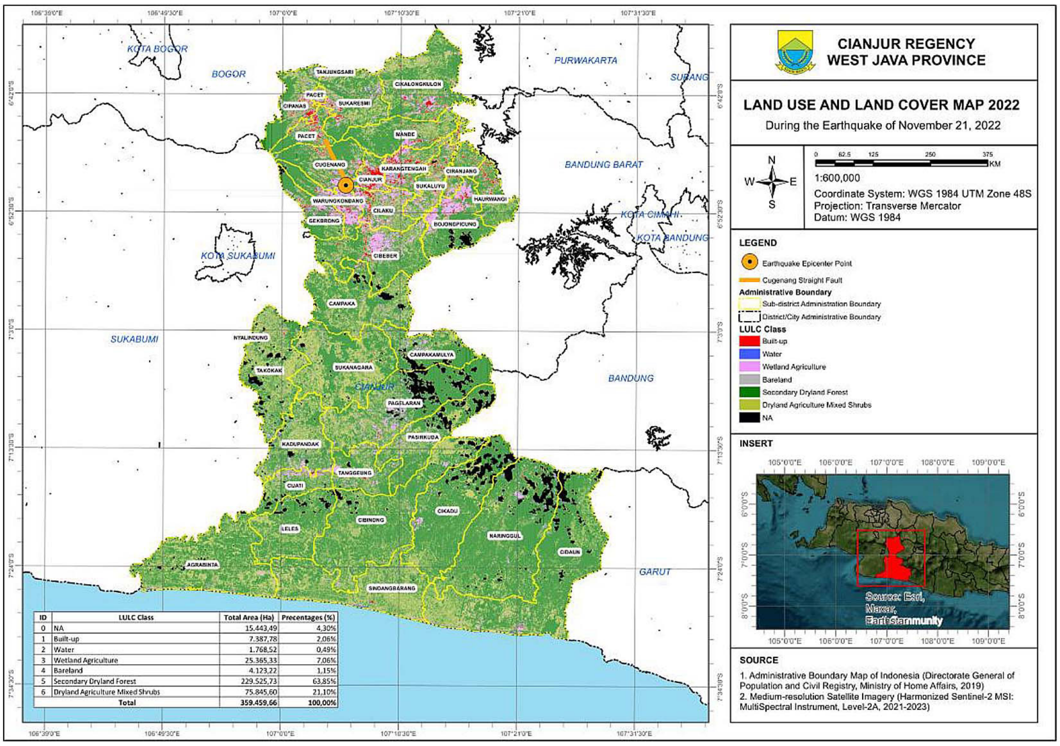

Figure 3. Land cover distribution in regency in 2022

Table 6. Land cover distribution in Cianjur Regency after the earthquake (2023)

ID	Land cover class	Area (ha)	Percentage (%)
0	No data (cloud/shadow)	0.01	0.00
1	Built-up land	34,437.11	9.58
2	Water bodies	799.46	0.22
3	Wet agricultural land	43,318.10	12.05
4	Open land	2,125.48	0.59
5	Secondary dryland forest	217,503.11	60.51
6	Mixed dryland agriculture and shrubland	61,275.83	17.05
Total		359,459.10	100.00

it formed extensive and relatively continuous vegetation cover. Mixed dryland agriculture and shrubland remained distributed within transition zones between forested and cultivated areas, whereas wet agricultural land was concentrated in relatively flat plains and valley areas in the northern and central parts of the study area.

One notable pattern observed in 2023 was the wider distribution of built-up land compared with previous years, particularly in the northern part of Cianjur Regency and along major settlement corridors. Meanwhile, open land occupied only a small proportion of the study area and was scattered across several locations. Overall, the 2023 map showed a landscape that remained dominated by vegetation and agricultural land, although the proportion of built-up land was greater than that observed before and during the earthquake.

Spatiotemporal dynamics of land cover (2021–2023)

A comparison of land cover conditions before (2021), during (2022), and after the earthquake (2023) revealed notable spatial and temporal changes across Cianjur Regency (Table 7). The largest changes were observed in secondary dryland forest, open land, built-up land, and wet agricultural land.

Secondary dryland forest, which represented the dominant land cover class, declined consistently from 236,170.58 ha in 2021 to 229,525.73

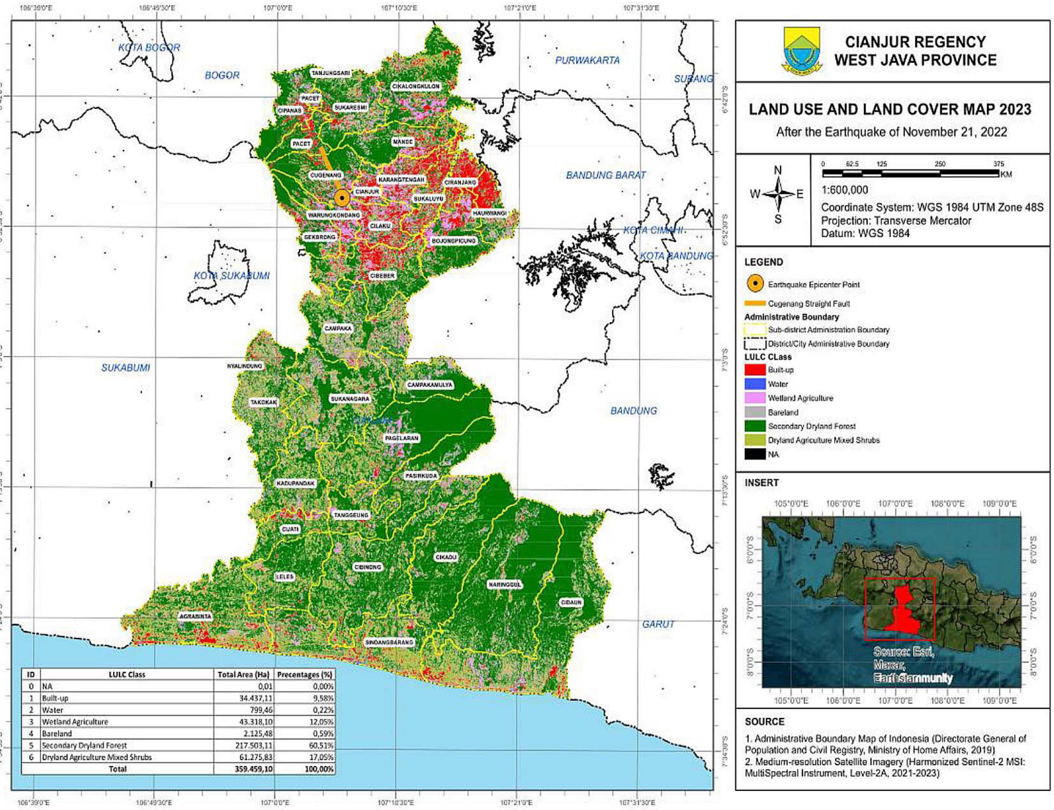

Figure 4. Land cover distribution in Cianjur Regency in 2023

Table 7. Land cover area and change rates in Cianjur Regency during 2021–2023

ID	Land cover class	Area (Ha)			Change 2021–2022 (%)	Change 2022–2023 (%)
		2021	2022	2023		
1	Built-up land	10,533.13	7,387.78	34,437.11	-29.86	366.14
2	Water bodies	1,151.40	1,768.52	799.46	53.60	-54.80
3	Wet agricultural land	39,471.04	25,365.33	43,318.10	-35.74	70.78
4	Open land	2,543.28	4,123.22	2,125.48	62.12	-48.45
5	Secondary dryland forest	236,170.58	229,525.73	217,503.11	-2.81	-5.24
6	Mixed dryland agriculture and shrubland	69,086.84	75,845.60	61,275.83	9.78	-19.21
Total		359,460.05	359,459.66	359,459.10		

Note: the cloud/shadow (no-data) class was excluded from the change-rate analysis because it does not represent an actual land-cover category.

ha in 2022 and further to 217,503.11 ha in 2023. Overall, the area of secondary dryland forest decreased by 18,667.47 ha, representing a reduction of approximately 7.9% during the study period. Open land exhibited the largest increase during the 2021–2022 period, expanding from 2,543.28 ha to 4,123.22 ha, equivalent to an increase of 62.1%. However, open land declined to 2,125.48 ha in 2023, representing a decrease of 48.5% compared with 2022. In contrast, built-up land decreased from 10,533.13 ha in 2021 to 7,387.78 ha in 2022 before increasing sharply to 34,437.11 ha in 2023. This increase corresponded to a 366.1% rise during the 2022–2023 period. Wet agricultural land also increased substantially, from 25,365.33 ha in 2022 to 43,318.10 ha in 2023, equivalent to a 70.8% increase.

Overall, land cover dynamics differed between the two observation periods. The 2021–2022 period was characterized by an expansion of open land and reductions in several vegetation classes, whereas the 2022–2023 period showed substantial increases in built-up land and wet agricultural land accompanied by a decline in open land. These patterns summarize the main land cover changes observed before, during, and after the 2022 earthquake.

DISCUSSION

Land cover classification reliability

The Random Forest algorithm produced satisfactory classification results across all observation years. Overall accuracy (OA) values reached 83.65%, 72.12%, and 75.00% for 2021, 2022, and 2023, respectively, while kappa coefficients ranged from 64.28% to 77.03%. Based on the classification proposed by Viera and Garrett (2005), all kappa values fell within the substantial agreement category, indicating good agreement between the classified maps and the reference data. These results suggest that the resulting land cover maps were sufficiently reliable for land cover change analysis.

The classification performance obtained in this study is consistent with findings reported in previous studies using Sentinel-2 imagery and the Random Forest algorithm for land cover mapping. Random Forest has been widely reported to achieve high classification accuracy because it can model complex spectral relationships and efficiently handle large numbers of predictor variables (Noi Phan et al., 2020; Patra et al., 2021). In addition, integrating spectral bands with vegetation, water, built-up land, and bare-land indices can improve class separability and thereby enhance classification accuracy (Sousa et al., 2020; Xing et al., 2021).

The class-specific accuracy assessment revealed variations among land cover classes. Secondary dryland forest consistently exhibited high classification accuracy throughout the study period, as reflected by its relatively high Producer's Accuracy and User's Accuracy values. The high accuracy of this class was likely associated with its distinctive spectral characteristics, particularly in the near-infrared (NIR) and shortwave infrared (SWIR) bands, which facilitate its separation from other land cover classes (Guo et al., 2020; Yasin et al., 2026). In addition, the spatial distribution of secondary dryland forest formed extensive patches with relatively low levels of fragmentation across much of central and southern Cianjur Regency. Such landscape characteristics reduce the occurrence of mixed pixels and contribute to more consistent classification results. Mixed pixels, which contain spectral information from multiple land cover types, are a major source of uncertainty in remote-sensing classification because they reduce class separability and increase the likelihood of misclassification. Therefore, the presence of large and relatively homogeneous forest areas likely contributed to the high classification accuracy observed in this study (Diniz et al., 2024; Panchal and Gupta, 2011).

In contrast, wet agricultural land exhibited relatively lower classification accuracy, particularly in 2022 and 2023. This condition was likely related to spectral similarities among wet agricultural land, mixed dryland agriculture and shrubland, and open land under different vegetation growth stages. Similar challenges in distinguishing agricultural land cover classes have been reported in previous Sentinel-2-based classification studies (Agapova et al., 2025). Furthermore, fragmented agricultural landscapes characterized by small and irregular land parcels pose challenges for accurate land cover classification. Such conditions increase the occurrence of mixed pixels and reduce the clarity of class boundaries, thereby increasing the potential for misclassification (Song et al., 2023)

Despite variations in classification accuracy among land cover classes and observation years, all land cover maps achieved accuracy levels generally considered adequate for regional-scale land cover analysis and change-detection studies. Therefore, the classification results can be considered a reliable basis for evaluating land cover dynamics in regency before, during, and after the 2022 Earthquake.

Land cover characteristics before the 2022 earthquake

The 2021 land cover distribution showed that the landscape of regency prior to the earthquake was dominated by vegetation cover, particularly secondary dryland forest and agricultural land. The dominance of these land cover classes reflects the physiographic characteristics of the region, which is largely composed of hilly and mountainous terrain that supports extensive forested and cultivated landscapes. This finding is consistent with the broader landscape characteristics of southern West Java, where forest and agricultural land remain dominant across upland and mountainous areas (BPBD Kabupaten, 2022; Shalih et al., 2023). The large proportion of vegetation cover indicates that ecological and agricultural functions constituted the primary components of the regional landscape before the earthquake.

Spatial analysis revealed that secondary dryland forest formed extensive and relatively continuous patches across the central and southern parts of regency. In contrast, agricultural land and settlements were more concentrated in the northern region and in areas with gentler topography. This pattern suggests a close relationship between topographic conditions and land-use distribution, whereby steeper areas tend to retain vegetation cover, whereas agricultural and settlement activities are concentrated in more accessible locations. Similar relationships between topography and land-use patterns have been widely reported in tropical mountainous regions, where terrain conditions and accessibility contribute to the persistence of vegetation cover on steeper slopes (Chen et al., 2025).

In addition to secondary dryland forest, mixed dryland agriculture and shrubland and wet agricultural land occupied substantial proportions of the landscape. The prominence of these agricultural classes highlights the importance of agriculture within the regional land-use system. The concentration of wet agricultural land in plains and valley areas indicates that agricultural activities are strongly influenced by topographic conditions and water availability. Such land-use configurations are commonly observed in rural Indonesian landscapes, where forests, agricultural land, and settlements form interconnected socio-ecological systems (Schepp et al., 2022; Wijaya, 2026).

Built-up land occupied only a small proportion of the study area and exhibited a clustered distribution around urban corridors and settlement centers. Notably, the epicentral area of the 2022 Earthquake was located in the northern part of the regency, where land cover was more heterogeneous than in the forest-dominated southern region. This finding indicates that the areas most directly affected by the earthquake consisted of a mosaic of settlements, agricultural land, and secondary vegetation. Previous studies have suggested that heterogeneous landscapes often exhibit more complex land-cover responses to major disturbances because of the close interaction between human activities and natural ecosystem components (Kang et al., 2022; P. Zhang et al., 2025).

Overall, the pre-earthquake landscape of regency was characterized by extensive vegetation cover and relatively low fragmentation of built-up areas. These baseline conditions provide an important reference for interpreting subsequent land-cover changes. Given that secondary dryland forest and agricultural land represented the dominant landscape components, changes in these classes were expected to play a major role in shaping landscape transformation during and after the 2022 earthquake.

Land cover changes during the earthquake, year 2022

The 2022 land cover classification revealed notable changes in landscape composition compared with pre-earthquake conditions. Although secondary dryland forest remained the dominant land cover class, its area declined together with wet agricultural land, while open land, water bodies, and mixed dryland agriculture and shrubland increased. These patterns suggest that the earthquake year represented an initial phase of landscape disturbance characterized by reductions in several vegetation classes and the expansion of disturbed land-cover categories.

The decline in secondary dryland forest observed in 2022 indicates that vegetation cover was among the landscape components affected during the disaster period. Previous studies have reported that the 2022 earthquake triggered hundreds of landslides across hilly and mountainous areas of the regency (Hadmoko et al., 2024; Zulfakriza et al., 2024). Landslides can remove vegetation through slope failure, tree damage, and the formation of exposed surfaces on affected hillsides. Furthermore, earthquake-induced geomorphological changes may alter slope stability and accelerate subsequent land-cover changes in environmentally sensitive areas.

The expansion of open land represented one of the clearest indicators of landscape disturbance during the earthquake year. This increase suggests a reduction in vegetation cover that had previously dominated much of the landscape. Several processes may have contributed to this pattern, including landslides, vegetation damage, emergency response activities, and post-disaster land-use adjustments. Similar responses have been documented in other earthquake- and landslide-affected regions, where vegetation disturbance is frequently accompanied by an increase in sparsely vegetated or unvegetated areas (Ihsan et al., 2023; Yang et al., 2018). Consequently, the expansion of open land may be interpreted as a spatial indicator of environmental disturbance associated with the earthquake.

Wet agricultural land also declined during 2022, suggesting that agricultural areas experienced landscape changes during the disaster year. Although this study did not directly evaluate agricultural productivity, the observed land-cover changes may reflect disruptions to both biophysical land conditions and cultivation activities. At the same time, the increase in mixed dryland agriculture and shrubland may indicate shifts in vegetation characteristics that altered the spectral response of some agricultural areas, resulting in their classification into different land-cover categories. These findings suggest that earthquake-related disturbances affected not only natural landscape components but also land-use systems associated with local livelihoods.

Despite these changes, secondary dryland forest and agricultural land continued to dominate the landscape structure of regency, accounting for more than 90% of the study area in 2022. This finding indicates that the overall landscape structure remained largely intact, although specific land-cover classes exhibited measurable changes. The expansion of open land and the reduction of several vegetation classes nevertheless demonstrate that the 2022 Earthquake influenced land-cover dynamics at the regional scale.

Overall, the 2022 landscape represented a transitional phase characterized by increasing open land and declining vegetation cover. The observed changes demonstrate that earthquake impacts can be detected not only through visible physical damage but also through shifts in land-cover composition captured by multitemporal remote-sensing data. This transitional phase provides an important basis for understanding subsequent landscape recovery and reorganization during the post-earthquake period.

Land cover changes after the earthquake (2023)

The 2023 classification results revealed a land cover composition that differed from that observed during the earthquake year. Although secondary dryland forest remained the dominant land cover class, its area continued to decline compared with previous years. In contrast, built-up land and wet agricultural land increased substantially, while the extent of open land decreased relative to 2022. These patterns suggest that post-earthquake land cover dynamics were increasingly influenced by landscape recovery and land-use reorganization rather than by direct environmental disturbance.

One of the most notable changes observed in 2023 was the expansion of built-up land to 34,437.11 ha, representing the largest land-cover change recorded during the study period. Although this study did not directly evaluate reconstruction programs or infrastructure development activities, the increase in built-up land may reflect post-disaster rehabilitation, reconstruction, and settlement expansion. Similar trends have been reported in other disaster-affected regions, where recovery processes are often accompanied by increased development activities and land-use change (Civelek et al., 2023; Kang et al., 2022).

Spatial analysis further revealed that the expansion of built-up land was not evenly distributed across regency. Most newly developed built-up areas were concentrated in the northern part of the regency, where settlements, economic activities, and transportation networks are predominantly located. In contrast, the central and southern regions remained largely dominated by secondary dryland forest and experienced comparatively limited changes. This pattern suggests that post-disaster landscape transformation was more pronounced in areas characterized by higher levels of human activity than in areas dominated by natural vegetation.

At the same time, open land decreased substantially compared with 2022. This reduction suggests that some of the open areas that emerged during the earthquake year transitioned into other land-cover classes. Such changes may be associated with natural revegetation processes as well as the reuse of land for agricultural and development activities. Similar reductions in open land following periods of disturbance have been reported in previous post-disaster studies, where affected landscapes gradually recovered through both ecological processes and human intervention (Bian et al., 2022; Wang et al., 2022). Consequently, the decline in open land observed in 2023 may be interpreted as an indicator of ongoing landscape reorganization following the disturbance that occurred in the previous year.

Wet agricultural land also increased substantially in 2023. The recovery of wet agricultural land compared with 2022 suggests that some previously disturbed areas were reused for cultivation activities. Although this study did not directly assess agricultural productivity, the observed increase may reflect the resumption of land-use activities by local communities following the disturbance phase. These findings indicate that post-disaster land-cover dynamics were influenced not only by environmental processes but also by human responses during the recovery period.

Despite these recovery-related changes, secondary dryland forest continued to decline through 2023. The persistent reduction in forest cover from the pre-earthquake period to the post-earthquake period suggests that some landscape changes were not fully reversed during the observation period. This finding highlights the possibility that environmental impacts associated with major disturbances may persist beyond the immediate disaster phase, particularly in landscapes vulnerable to vegetation-cover change.

Overall, the 2023 landscape represented a phase of post-disaster reorganization characterized by expanding built-up land and wet agricultural land, declining open land, and a continued reduction in forest cover. Together, these patterns indicate that post-earthquake land-cover dynamics reflected both environmental recovery processes and ongoing adjustments in land use during the recovery period.

Spatiotemporal dynamics of land cover before, during, and after the 2022 earthquake

The multitemporal analysis revealed that land cover change in Cianjur Regency occurred gradually and followed two broad stages during the observation period. The first stage, spanning 2021–2022, was characterized by an expansion of open land and reductions in several vegetation classes, particularly secondary dryland forest and wet agricultural land. This pattern is consistent with a disturbance period associated with environmental impacts occurring during the earthquake year. The second stage, covering 2022–2023, was characterized by increases in built-up land and wet agricultural land accompanied by a decline in open land. These changes suggest a period of landscape reorganization in which some previously affected areas were reused and incorporated into new land-use activities.

One of the most important findings of this study is that landscape transformation did not cease during the earthquake year. Secondary dryland forest declined continuously from 236,170.58 ha in 2021 to 217,503.11 ha in 2023, representing a reduction of approximately 7.9% over the observation period. The persistent decline suggests that some landscape changes were not entirely temporary. In mountainous environments, post-disaster vegetation change is often influenced by a combination of geomorphological processes, vegetation disturbance, and subsequent land-use change (Yang et al., 2018; Hadmoko et al., 2024). Accordingly, the environmental consequences of earthquakes may extend beyond the immediate disaster period and continue during subsequent years.

Another notable finding was the shift in land-cover composition between the earthquake year and the post-earthquake period. The year 2022 was characterized by increasing open land and declining vegetation cover, whereas 2023 showed substantial increases in built-up land and wet agricultural land together with a reduction in open land. These contrasting patterns suggest that post-earthquake landscape dynamics were influenced not only by environmental disturbances associated with the disaster but also by recovery-related processes that occurred afterwards. The expansion of built-up land and the recovery of wet agricultural land may reflect the reuse of affected areas through reconstruction, rehabilitation, and renewed productive activities. Therefore, post-earthquake landscape transformation can be viewed as the result of interactions between natural disturbance processes and human responses during the recovery period (J. Zhang et al., 2025).

The findings also demonstrate the value of a multitemporal approach for assessing post-disaster environmental change. A conventional before–after analysis based on only two observation periods would have been unable to clearly capture the transitional conditions that emerged during the earthquake year and the subsequent changes that occurred during recovery. By incorporating multiple observation periods, the present study was able to identify gradual changes in landscape composition and provide a more comprehensive understanding of the direction and magnitude of post-disaster landscape transformation at the regional scale (Vu & Kamthonkiat, 2016).

Overall, the results suggest that land-cover change associated with the 2022 earthquake occurred through two broad stages: an initial disturbance stage during the earthquake year and a subsequent landscape reorganization stage during the post-disaster period. These findings highlight that earthquake-related environmental impacts are reflected not only in immediate landscape disturbance but also in longer-term processes of recovery and land-use adjustment. Consequently, multitemporal monitoring is important for environmental impact assessment, landscape rehabilitation planning, and geospatially informed disaster risk reduction strategies.

CONCLUSIONS

The results showed that land-cover changes were not limited to the earthquake year but continued throughout the post-earthquake period. During the observation period, secondary dryland forest declined consistently, while open land increased during the earthquake year and subsequently decreased in the following year. In contrast, built-up land and wet agricultural land expanded during the post-earthquake period.

The findings revealed that post-disaster land-cover dynamics occurred through two broad phases: a disturbance phase characterized by increasing open land and declining vegetation cover during the earthquake year, followed by a reorganization phase characterized by the expansion of built-up land and wet agricultural land during the recovery period. These patterns suggest that post-earthquake landscape transformation was shaped by interactions between environmental disturbance and human responses during recovery.

The novelty of this study lies in the application of a multitemporal approach to evaluate land-cover dynamics across three distinct phases: before, during, and after the earthquake. Unlike conventional before–after analyses, this approach captured transitional landscape conditions and longer-term post-disaster changes. The findings contribute to a more comprehensive understanding of post-disaster landscape transformation and provide geospatial evidence that may support environmental rehabilitation, spatial planning, and disaster risk reduction efforts.

Acknowledgments

The authors would like to express their sincere gratitude to their supervisors for their invaluable guidance, constructive feedback, and continuous encouragement throughout this research. Their expertise and support greatly contributed to the development and completion of this study.

The authors also acknowledge Universitas Esa Unggul and Universitas Sebelas Maret for providing academic support, research facilities, and institutional assistance that facilitated the successful conduct of this research.

REFERENCES

1. Adugna, T., Xu, W., Fan, J. (2022). Comparison of random forest and support vector machine classifiers for regional land cover mapping using coarse resolution FY-3C images, *Remote Sensing, 14*(3), 574. https://doi.org/10.3390/rs14030574
2. Agapova, E. R., Medvedeva, M. A., Karlson, M., Bastviken, D. (2025). Monitoring of flooded vegetation of rewetted peatlands based on remote sensing data, *Journal of Geophysical Research: Biogeosciences*, *22*(6), 337–349. https://doi.org/10.21046/2070-7401-2025-22-6-337-349
3. Arwasaputra, L. T., Setiawan, M. R., Sugiarto, B., Permanasari, I. N. P., Pardede, I. (2024). Geophysical investigation of the 2022 earthquake: Uncovering a new active fault. *International Seminar of Science and Applied Technology: Natural Resources Management for Environmental Sustainability (ISSAT 2023)*, *479*(E3S Web of Conf.), 02008. https://doi.org/10.1051/e3sconf/202447902008
4. Awaluddin, M. (2026). Coseismic deformation of the indonesian geospatial reference system 2013 from the 2022 Earthquake. *International Journal of Geoinformatics*, *22*(5), 144–155. https://doi.org/10.52939/ijg.v22i5.4985
5. Benson, N., Carl H, K. (2006). *Landscape assessment: Ground measure of severity, the composite burn index; and remote sensing of severity, the normalized burn ratio*. In: D.C. Lutes, R.E. Keane, J.F. Caratti, et al. (Eds) Fire Effects Monitoring and Inventory System. Publisher: USDA Forest Service, Rocky Mountain Research Station, Ogden, UT.
6. Bian, Z., Zhang, D., Xu, J., Tang, H., Bai, Z., Li, Y. (2022). Study on the evolution law of surface landscape pattern in Earthquake-Stricken areas by remote sensing: A case study of Jiuzhaigou County, Sichuan Province. *Sustainability (Switzerland)*, *14*(20). https://doi.org/10.3390/su142013032
7. BPBD Kabupaten (2022). *Kajian Risiko Bencana Kabupaten Tahun 2018–2022*.
8. Caja, C. C., Ibunes, N. L., Paril, J. A., Reyes, A. R., Nazareno, J. P., Monjardin, C. E., Uy, F. A. (2018). Effects of Land Cover Changes to the Quantity of Water Supply and Hydrologic Cycle Using Water Balance Models. *MATEC Web of Conferences*, *150*, 1–4. https://doi.org/10.1051/matecconf/201815006004

9. Chen, K., Zhang, Y., Wang, X., Liu, X., Hu, R., Lei, X., Fan, Q. (2025). Coupled effects of slope and vegetation cover characteristics on hydrodynamic erosion forces and sediment yield processes in the southern Ningxia mountainous area. *Arid Zone Research*, *42*(11), 2044–2057. https://doi.org/10.13866/j.azr.2025.11.08
10. Civelek, N., Inalpulat, M., Genc, L. (2023). Evaluation of earthquake impacts on land use and land cover (LU/LC) using google earth engine (GEE), Sentinel-2 imageries, and machine learning: case study of Antakya. *Journal of Anatolian Environmental and Animal Sciences*, *4*, 642–650. https://doi.org/https://doi.org/10.35229/jaes.1349826
11. Diniz, É. S., Mota, P. H. S., Reis, J. P., da Silva Costa, W., de Paiva, E. V, de Lana, J. M., Lage, G. B., do Amaral, C. H. (2024). Connectivity value of Atlantic forest fragments: pathways towards enhancing biodiversity conservation. *Revista Brasileira de Botanica*, *47*(1), 249–259. https://doi.org/10.1007/s40415-023-00970-0
12. Guo, Y., Li, Z., Chen, E., Zhang, X., Zhao, L., Chen, Y., Wang, Y. (2020). A deep learning method for forest fine classification based on high resolution remote sensing images: two-branch FCN-8s. *Linye Kexue/Scientia Silvae Sinicae*, *56*(3), 48–60. https://doi.org/10.11707/j.1001-7488.20200306
13. Hadmoko, D. S., Wibowo, S. B., Sianipar, D. S. J., Daryono, D., Fathoni, M. N., Pratiwi, R. S., Haryono, E., Lavigne, F. (2024). Co-seismic deformation and related hazards associated with the 2022 Mw 5.6 earthquake in West Java, Indonesia: insights from combined seismological analysis, DInSAR, and geomorphological investigations. *Geoenvironmental Disasters*, *11*(1). https://doi.org/10.1186/s40677-024-00277-6
14. Handoyo, F. W., Dalimunthe, S. A., Purwanto, Suardi, I., Yuliana, C. I., Mychelisda, E., Wardhana, I. W., Nugroho, A. E. (2024). Enhancing disaster resilience: Insights from the earthquake to improve indonesia's risk financing strategies. *Sage Open*, *14*(2), https://doi.org/10.1177/21582440241256777
15. Ihsan, M., Marnani, C. S., Bahar, F. (2023). Build back better: Rehabilitation and reconstruction after the earthquake disaster. *International Journal of Progressive Sciences and Technologies (IJPSAT*, *38*(1), 435–441.
16. Indonesian Ministry of Environment and Forestry. (2020). *Technical Guidelines of the Directorate of Forest Resource Inventory and Monitoring*.
17. Kang, J., Wang, Z., Cheng, H., Wang, J., Liu, X. (2022). Remote sensing land use evolution in earthquake-stricken regions of Wenchuan county, China. *Sustainability (Switzerland)*, *14*(15). https://doi.org/10.3390/su14159721
18. Li, S., Chen, X. (2014). A new bare-soil index for rapid mapping developing areas using Landsat 8 data. *International Archives of the Photogrammetry, Remote Sensing and Spatial Information Sciences - ISPRS Archives*, *40*(4), 139–144. https://doi.org/10.5194/isprsarchives-XL-4-139-2014
19. Liu, H. Q., Huete, A. (1995). A feedback based modification of the NDVI to minimize canopy background and atmospheric noise. *IEEE Transactions On Geoscience And Remote Sensing 33* (2).
20. Mashala, M. J., Dube, T., Mudereri, B. T., Ayisi, K. K., Ramudzuli, M. R. (2023). A systematic review on advancements in remote sensing for assessing and monitoring land use and land cover changes impacts on surface water resources in semi-arid tropical environments. *Remote Sensing*, *15*(16). https://doi.org/10.3390/rs15163926
21. Noi Phan, T., Kuch, V., Lehnert, L. W. (2020). Land cover classification using google earth engine and random forest classifier-the role of image composition. *Remote Sensing*, *12*(15). https://doi.org/10.3390/RS12152411
22. Panchal, V. K., Gupta, N. (2011). Swarm intelligence for mixed pixel resolution. *Recent Researches in Telecommunications, Informatics, Electronics and Signal Processing – TELE-INFO'11, MINO'11, SIP'11*, 24–28.
23. Patra, S. S., Jena, O. P., Kumar, G., Pramanik, S., Misra, C., Singh, K. N. (2021). Random Forest Algorithm in Imbalance Genomics Classification. In: *Data Analytics in Bioinformatics: A Machine Learning Perspective*, 173–190. https://doi.org/10.1002/9781119785620.ch7
24. Phiri, D., Simwanda, M., Salekin, S., Nyirenda, V. R., Murayama, Y., Ranagalage, M. (2020). Sentinel-2 data for land cover/use mapping: a review. *Remote Sensing Journal*, *12*. https://doi.org/10.3390/rs12142291
25. Prayogo, M. A. (2023). Analysis of land cover and building damage due to the 21th November 2022 earthquake using Sentinel-2. *IOP Conference Series: Earth and Environmental Science*, *1276*(1). https://doi.org/10.1088/1755-1315/1276/1/012037
26. Schepp, C., Diekkrüger, B., Becker, M. (2022). Hillslope hydrology in a deeply weathered saprolite and associated nitrate transport to a valley bottom wetland in central Uganda. *Hydrology*, *9*(12). https://doi.org/10.3390/hydrology9120229
27. Shalih, O., Adi, A. W., Wiguna, S., Shabrina, F. Z., Syauqi, Hafizh, A., Iftidah, A., Dewi, A. N. (2023). *RBI (Risiko Bencana Indonesia) 2023 'Memahami Risiko Sistemik di Indonesia'*.
28. Sidle, R. C., Gomi, T., Akasaka, M., Koyanagi, K. (2018). Ecosystem changes following the 2016 Kumamoto earthquakes in Japan: Future perspectives. *Ambio*, *47*(6), 721–734. https://doi.org/10.1007/s13280-017-1005-8

29. Song, W., Wang, C., Mu, X., Fang, G., Wang, H., Zhang, H., Dong, T., Wang, Z., Wang, C., Mu, X., Zhang, H. (2023). Hierarchical extraction of cropland boundaries using Sentinel-2 time-series data in fragmented agricultural landscapes. *2023 11th International Conference on Agro-Geoinformatics, Agro-Geoinformatics 2023*, *212*. https://doi.org/10.1109/Agro-Geoinformatics59224.2023.10233358
30. Sousa, C. De, Fatoyinbo, L., Neigh, C., Boucka, F., Angoue, V., Larsen, T. (2020). Cloud-computing and machine learning in support of country-level land cover and ecosystem extent mapping in Liberia and Gabon. *PLoS ONE*, *15*(1). https://doi.org/10.1371/journal.pone.0227438
31. Viera, A. J., Garrett, J. M. (2005). Understanding interobserver agreement: the kappa statistic. *Family Medicine*, *37*(5), 360–363.
32. Vu, T.-T., Kamthonkiat, D. (2016). Monitoring long-term disaster recovery – space and ground views. In: *Remote Sensing and Digital Image Processing 20*, 427–445. https://doi.org/10.1007/978-3-319-47037-5_20
33. Wang, J., Wang, Z., Cheng, H., Kang, J., Liu, X. (2022). land cover changing pattern in pre- and post-earthquake affected area from remote sensing data: a case of Lushan County, Sichuan Province. *Land 11*(8), 1205. https://doi.org/10.3390/land11081205
34. Wijaya, A. (2026). Exploring spatiotemporal patterns of agricultural land-use change in Banyuwangi Regency using GIS-based analysis. *IOP Conference Series: Earth and Environmental Science*, *1595*(1). https://doi.org/10.1088/1755-1315/1595/1/012036
35. Xing, H., Zhu, L., Niu, J., Chen, B., Wang, W., Hou, D. (2021). A land cover change detection method combing spectral values and class probabilities. *IEEE Access*, *9*, 83727–83739. https://doi.org/10.1109/ACCESS.2021.3087206
36. Xu, H. (2006). Modification of normalised difference water index (NDWI) to enhance open water features in remotely sensed imagery. *International Journal of Remote Sensing*, *27*(14), 3025–3033. https://doi.org/10.1080/01431160600589179
37. Yang, W., Qi, W., Zhou, J. (2018). Decreased post-seismic landslides linked to vegetation recovery after the 2008 Wenchuan earthquake. *Ecological Indicators*, *89*, 438–444. https://doi.org/10.1016/j.ecolind.2017.12.006
38. Yasin, E. H. E., Koreň, M., Czimber, K. (2026). Machine learning-based mapping of dominant tree species in dryland forests using multi-temporal and multi-source data. *Remote Sensing*, *18*(8). https://doi.org/10.3390/rs18081185
39. Zha, Y., Gao, J., Ni, S. (2003). Use of normalized difference built-up index in automatically mapping urban areas from TM imagery. *International Journal of Remote Sensing*, *24*(3), 583–594. https://doi.org/10.1080/01431160304987
40. Zhang, J., Zhang, Y., Dannenberg, M. P., Guo, Q., Atkins, J. W., Li, W., Sun, G. (2025). Eco-hydrological recovery following large vegetation disturbances from a mega earthquake on the eastern Tibetan plateau. *Journal of Hydrology*, *651*. https://doi.org/10.1016/j.jhydrol.2024.132595
41. Zhang, P., Tang, X., Yang, Z., Zhou, T., Fu, S., Wang, S., Luo, K. (2025). Analysis of land use change and landscape pattern in Luding County after the MS6.8 earthquake based on machine learning. *Journal of Natural Disasters*, *34*(3), 59–77. https://doi.org/10.13577/j.jnd.2025.0306
42. Zulfakriza, Z., Nugraha, A. D., Heryandoko, N., Ry, R. V., Muttaqy, F., Andika, A., Azhari, M. F., Putra, A. S., Palgunadi, K. H., Cummins, P. R., Supendi, P., Lesmana, A., Sahara, D. P., Puspito, N. T. (2024). Seismic source analysis of the destructive earthquake November 21, 2022, Mw 5.6 (Indonesia) from relocated aftershock. *Scientific Reports*, *14*(1), 12142. https://doi.org/10.1038/s41598-024-60408-9